Published by IOP Publishing for Sissa Medialab

Received: *September 23, 2025*
Accepted: *November 23, 2025*
Published: *December 10, 2025*

Secondary radiation measurements from Moon regolith simulant and aluminum targets in collision with 430 MeV/u proton, helium and carbon ions

A. Sokolov,[a,*] **E. Kozlova,**[a] **D. Boscolo,**[a] **A. Di Chicco,**[b] **F. Luoni,**[a,c] **T. Radon,**[a] **C. Schuy,**[a] **T. Wagner,**[a] **U. Weber**[a,d] **and M. Zboril**[b]

[a] *GSI Helmholtz Center for Heavy Ion Research, Darmstadt, Germany*
[b] *Physikalisch-Technische Bundesanstalt, Braunschweig, Germany*
[c] *Technische Universität Darmstadt, Darmstadt, Germany*
[d] *Technische Hochschule Mittelhessen, Gießen, Germany*

E-mail: Al.Sokolov@gsi.de

Abstract: In this study aluminum and Moon regolith (substitute) materials were irradiated at HIT medical facility with protons, helium and carbon ions, at energy 430 MeV/u. The ambient doses equivalent — $H^*(10)$ values were measured with different equipment at different angles relative to the target(s) and compared with simulations done using Monte Carlo code — FLUKA. The measured doses showed a good agreement with FLUKA simulations; different aspects of the measured radiation fields, as well as of the used measurement equipment are discussed.

Keywords: Radiation calculations; Detector modelling and simulations I (interaction of radiation with matter, interaction of photons with matter, interaction of hadrons with matter, etc); Models and simulations

*Corresponding author.

https://doi.org/10.1088/1748-0221/20/12/P12014

2025 JINST 20 P12014

Contents

1 Introduction **1**

2 Material and methods **2**
- 2.1 Measurement equipment 2
- 2.2 Targets and beam parameters 4
- 2.3 Monte Carlo simulations 4

3 Experimental results and discussion **5**
- 3.1 Raster scans 5
- 3.2 Moon regolith target 6
- 3.3 Aluminum target 9

4 Summary **12**

1 Introduction

Radiation protection studies require reliable measuring equipment and are nowadays supported additionally by radiation field modelling tools, which simplify these studies. Simulations of radiation effects help in complicated direct measurement cases, as deep under the earth, in nuclear reactors or in space. Still the codes should be continuously cross checked with the experimental results. Vice versa, the measurements with radiation detectors can reveal unpredicted results, which could be explained using simulations.

The typical dosimeters used at accelerator complexes like GSI [1] are pretty precise, but also quite heavy devices, thus their usage e.g., in space is not desirable. For neutron monitoring the passive GSI ball [2] and active ThermoFisher‘s Wendi-II [3] dosimeters are used. The ionizing radiation is typically measured with the passive GSI cylinder [4] dosimeter and Ionization Chamber FHT192, also from ThermoFisher [5]. Both passive dosimeters have ThermoFisher's TLD600 or TLD700 cards as sensitive elements, which are normally read-out after the measurements with a special TLD-Reader. All this heavy equipment will not likely appear for example on the Moon in next decades. Still the ambient dose equivalent measurements with Moon regolith under irradiation with most abundant particles in galactic cosmic radiation (GCR) can be performed already now on earth, during experiments at the heavy ion accelerator facility.

The Monte Carlo code FLUKA [6, 7] is used at GSI for radiation protection simulations: to estimate the necessary shielding or activation of the beam line components. FLUKA is well-known tool for radiation protection, medical application and space research calculations, benchmarked against big varieties of experiments.

In our studies we used a Moon regolith substitute and aluminum targets, which were irradiated at HIT facility [8] with protons, ^{4}He and ^{12}C ions. The ambient doses were measured with our commonly used equipment and the results were compared with FLUKA simulations. Additionally numerous simulations were performed to check the responses of the used dosimeters.

2025 JINST 20 P12014

One should also mention, that in the frame of the same experiment, the neutron spectra [9] and the depth-dose curves [10] for the different shielding materials were measured. Both articles can provide an additional information and more details on the experiment.

2 Material and methods

2.1 Measurement equipment

GSI ball passive dosimeter has a response function close to the neutron fluence-to-ambient dose conversion, which was tested at PTB [11] and approved by us at different experiments [12, 13]. As it was mentioned the sensitive element of this passive equipment is a Thermo Luminescence Detector (TLD) card, with 2 TLD600 and 2 TLD700 crystals, placed in the middle of the moderator sphere made of high-density polyethylene with a lead layer insertion. The TLD700 crystals with Li-7 element allow for gamma and charged particles detection, whereas TLD600 with Li-6 allows additionally for neutron detection, due to ^{6}Li(n, t)^{4}He reaction. The difference between TLD600 and TLD700 signals is proportional to the neutron ambient dose, which with a calibration using standard ^{241}Am-Be(α, n) neutron source gives us an estimate or measured ambient dose equivalent value. Our previous measurements at high energetic radiation fields [14] showed that there is an additional neutron signal readout for the measurements at small angles relative to the beam direction, which appears due to the high energetic secondary proton interaction with the PE sphere. That means that special corrections should be applied to the measurements to obtain the true neutron ambient dose equivalent, related only to the neutron radiation field.

GSI cylinder passive dosimeter is also a well-tested equipment used by us in numerous experiments. The sensitive element in that case is a TLD card containing TLD700 crystals only, as the dosimeter is used for gammas and charged particles detection. The dosimeter is calibrated by us using standard Cs-137 gamma source. Numerous simulations were performed to calculate the response functions of the GSI cylinder to different particles, like muons, pions, etc. In figure 1 the responses to photons, protons and carbon ions are presented.

Additionally, to the standard cylindrical dosimeter, which is a solid cylinder 5 cm in diameter and 6 cm in height, another design with 3 TLDs was used. In that case the dosimeter was in a shape of a cylindrical capsule with overall wall thickness of 1 cm, inside which the TLDs were placed to form a triangle. This design improves the response function for protons around 20–40 MeV and for high energy gammas, as the thickness of PE is less in comparison to a solid form.

Wendi-II dosimeter from ThermoFisher is a world-famous neutron rem counter with a He-3 counter tube centered in PE moderator with insertion of a tungsten layer. As well as GSI ball dosimeter, Wendi-II is designed for wide neutron energy range. The response function of Wendi-II in comparison to GSI ball response and Pellicioni [15] conversion coefficients for neutron $H^{*}(10)$ ambient dose can be found in figure 2.

The Wendi-II was used in combination with ThermoFisher's nitrogen filled Ionization Chamber FHT191N [16], another PTB approved device for gamma dose measurements. Both probes were connected to FHT6020 electronics remotely controlled over Ethernet, from which the dose rates history values were read out every minute for neutron and 30 seconds for gamma probes, respectively.

2025 JINST 20 P12014

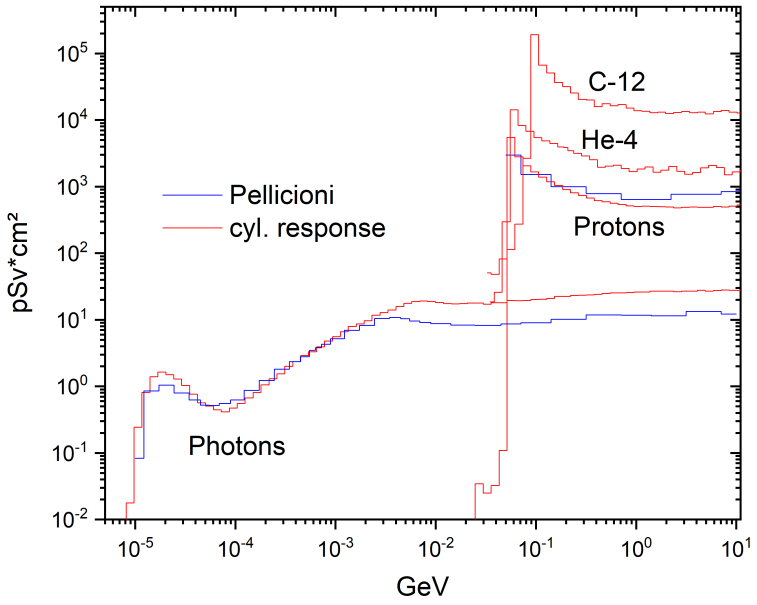

Figure 1. Fluence-to-ambient dose conversion coefficients, according to Pellicioni [15], and response functions of the cylinder TLD dosimeter for photon, proton, helium and carbon beams.

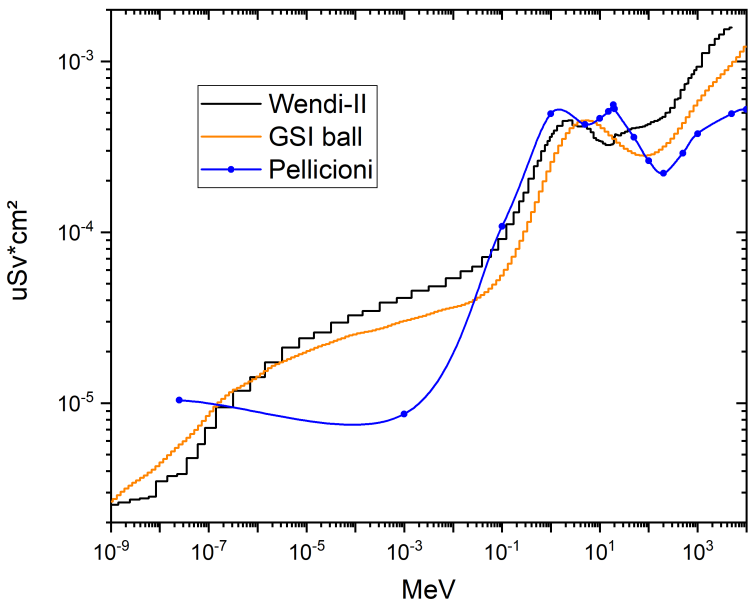

Figure 2. Neutron $H^*(10)$ values according to Pellicioni [15] and response functions of the GSI ball dosimeter in comparison to Thermo Fisher's Wendi-II dosimeter.

2025 JINST 20 P12014

2.2 Targets and beam parameters

The experiment was performed at Heidelberger Ionenstrahl-Therapiezentrum (HIT) which is an operational medical facility for cancer therapy. The facility also possesses an experimental room for different kind of research with protons, helium, carbon and oxygen beams. These ion species are interesting for the space research as they are the primary components of cosmic radiation. As it is given in [17] the protons are the most abundant with 90 %, followed by the alpha particles with around 7 % and then C, N, O at around 1 % of the GCR flux. In the present experimental campaign beam intensities of around 10^9 particles per spill for He and carbon ions, and around 10^{10} protons per spill were used, sufficient to accumulate the necessary dose for the passive dosimeters.

Initially the passive gamma cylinders were irradiated directly with protons and helium ions at 200 MeV/u to test the response function of the dosimeters. During the main experiment, we focused on proton, helium and carbon beams at 430 MeV/u, which is close to the proton and helium energy peak in the GCR spectrum [18]. The most relevant materials for a Moon mission were irradiated, namely aluminum, which is a major spacecraft construction material and lunar regolith, represented in this experiment by a Moon regolith simulant [17], having an atomic composition close to the real material. In particular, we used the OPRH2N Near-Side Highland Lunar regolith simulant from Off Planet Research [19], with a customized granular structure of 250–500 microns. This material was already used in several simulation and experimental studies [10, 20]. The lunar simulant with a density of 1.345 g/cm^3 was filled into plastic boxes with inner dimensions $10 \times 23 \times 23$ cm^3. The boxes were not filled completely and had slightly different filling ratios. On average for simulations the height of 18.5 cm of Moon regolith substitute material was used to take into account the voids in the box, the rest was filled with air. The target is a stack of 9 boxes providing moon target thickness of approximately 90 cm, which should be enough to stop completely the 430 MeV primary proton beam, as it's range in the target is around 85 cm. The Aluminum target is a stack of 30×30 cm^2 blocks of different thicknesses (30 and 25 mm) with a total thickness of 50 cm. The material is $AlMg_3$ alloy of 2.65 g/cm^3 density with magnesium mass fraction of 3.5 %. Stopping range of 430 MeV protons in this type of target is only around 46 cm, as the effective atomic number and density is higher in comparison to the Moon regolith simulant.

2.3 Monte Carlo simulations

Numerous simulations for the experiment were performed with FLUKA. In particular the $H^*(10)$ values at different positions around the target, irradiated by the primary beams of the mentioned ion species, were calculated with the full HIT experimental room geometry included. In the simulations the beam was assumed to have a gaussian shape with FWHM of 1 cm, which is a realistic assumption, though it was not measured directly during the experiment. For this work the FLUKA version fluka2023.3 was used, the geometries for the experimental setup and detectors layouts were build using FLAIR [21]. Until 2023 the FLUKA was using Pellicioni's fluence-to-ambient dose conversion coefficients only for photons, neutrons, protons, electrons/positrons and few other charged particles like pions and muons. Since then, additional conversion coefficients have been implemented for alpha particles and, as stated in FLUKA manual (http://www.fluka.eu), a "very crude attempt" has been made to apply ambient dose conversion coefficients to ions, "rescaling from available ones". That means that starting from 2023, the conversion coefficients are also applied to the helium and carbon

2025 JINST 20 P12014

ions used in our experiment, and simulations can provide the total ambient dose equivalent values, although FLUKA can also distinguish the contribution from different particles as well.

FLUKA simulations of the dosimeters' responses, were made in a simple geometry irradiating detectors, i.e.: neutron spheres and gamma cylinders with parallel monoenergetic beams. For the cylinders, the energy deposition in TLD700 crystals was scored and normalized to energy deposition from 661 keV photons, which is the energy of the ^{137}Cs gamma source used for dosimeters calibration. For neutron spheres the signal is obtained as a difference between absorbed energy in TLD600 and in TLD700 crystals. The spheres were irradiated in simulations with neutrons of AmBe source spectrum and the signal from monoenergetic neutrons was normalized to the signal from AmBe source, which is used for calibration of the neutron dosimeters.

3 Experimental results and discussion

3.1 Raster scans

The medical facilities have an advantage of precise adjustment of the beam dose, required for therapy. This feature was used to test GSI passive cylinder dosimeters and our simulation approach for response calculation with FLUKA. The raster scanning technique was used for carbon, helium and proton beams to irradiate a square pattern of $15 \times 15\,\mathrm{cm}^2$, with fluences adjusted to provide 0.1 Gy of "dose in water", which is the energy loss of the beam in 1 cm water thickness. In table 1, one can see the measured and expected from simulation ambient dose values, along with the direct conversion of ion fluences into ambient dose using the coefficients from FLUKA. The uncertainties of up to 10 % for the measurement results are expected, that's why the doses are given only up to the 2$^{\mathrm{nd}}$ digit after the comma. The ambient doses from simulations, calculated using absorbed energy for scoring, as described in section 2.3, are very close to the measured values, though the discrepancy for proton with overestimation and for carbon beams with underestimation, could point out to the necessity of a bit more sophisticated method of the cylinders' response calculations. Also, the "improved" design of the passive cylindrical dosimeter with 3 TLD cards showed measured values very close to those of single-card dosimeters. The direct ion fluence-to-ambient dose conversion in FLUKA showed higher values, especially for heavier carbon ions. Based on direct irradiation, we estimate the precision of our ambient dose measurements for light ions using GSI passive cylinder dosimeter to be within 30 % relative to the expected values. For photons and electrons, as well as for other charged particles like muons, the response of the dosimeter should be much better [4]. In the main experiment the standard cylindrical dosimeters with a single TLD card were used.

Table 1. Result of the ambient dose measurements with passive cylindrical dosimeters using raster scan, providing 0.1 Gy of "dose in water", and comparison to the simulation results of the dosimeter response and direct scoring of $H^*(10)$ values in FLUKA.

	Energy [MeV/u]	ions [1/cm^2]	Dose in water [Gy]	simulated response Cyl. 1 TLD [Sv]	simulated response Cyl. 3 TLD [Sv]	measured amb. dose Cyl. 1 TLD [Sv]	measured amb. dose Cyl. 3 TLD [Sv]	$H^*(10)$ FLUKA sim. [Sv]
p	200	1,4E+08	0,10	**0,11**	**0,11**	**0,14**	**0,14**	0,15
He-4	200	3,5E+07	0,10	**0,12**	**0,11**	**0,12**	**0,12**	0,15
C-12	430	5,9E+06	0,10	**0,08**	**0,10**	**0,07**	**0,07**	0,17

2025 JINST 20 P12014

3.2 Moon regolith target

The experimental setup modelled using FLAIR can be seen in figure 3 (left), which depicts the experimental cave with the target, described in section 2.2, and five positions around the target. The positions are located at the height of the beam line in vertical direction and in horizontal plane at: 0°, 12°, 26°, 39°, 90° angles, relative to the beam direction, and at distances: 235 cm, 230 cm, 245 cm, 230 cm, 195 cm, relative to the front end of the target, respectively. The positions were kept constant during experiment and only the target was exchanged. As the moon and Al targets have different heights: 18.5 and 30 cm, respectively, their vertical positions were adjusted for the beam to hit the centre of each target. Additionally, for helium beam the cylindrical dosimeters were placed not only around, but also on top of the targets.

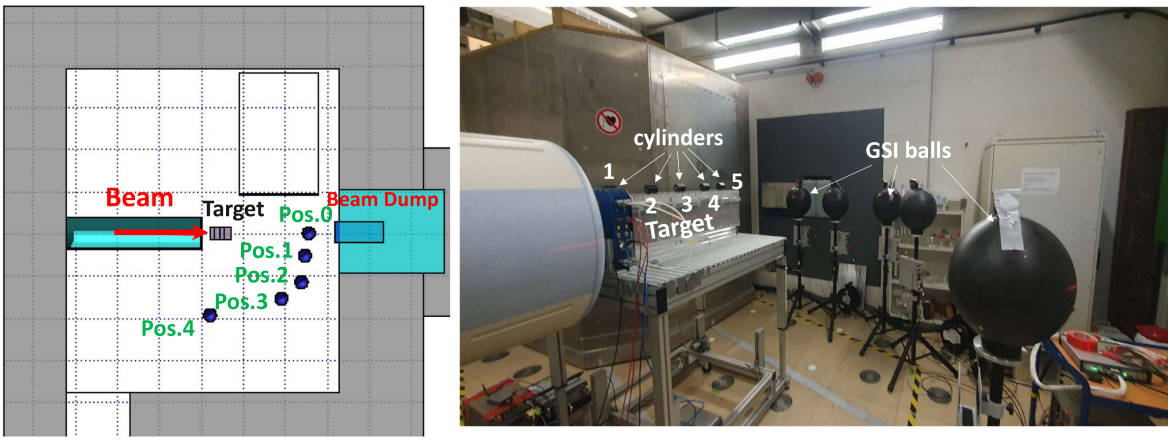

Figure 3. Experimental setup modelled using FLAIR interface (left) and the photo of the HIT experimental room (right). The beam comes from the left to the right and hit the target, on which the cylinder dosimeters are placed. Around the target there are 5 positions to put active or passive dosimeters for the ambient dose measurements.

In table 2 one can find measured with GSI ball the neutron ambient dose equivalent (2nd row) and calculated according to ICRP74 using FLUKA the $H^*(10)$ values (3rd row) at different positions around the moon target. The neutron ambient dose values are for 20 spills of 430 MeV protons, which corresponds to 1.78e11 beam particles delivered to the target. The next (4th) row in the table presents the ratio of the mentioned experimentally measured values to the corresponding FLUKA-simulated results. The subsequent (5th) row shows the ratio between the neutron ambient dose equivalents measured with the active Wendi-II dosimeter and the values obtained from the FLUKA simulations. Unlike the measurements with passive dosimeters, which were positioned once and for which only the TLD cards were exchanged for different ion beams, the active dosimeters were first positioned at a certain point, irradiated in different beams and then moved to another position. Thus, in the fifth row of table 2 with the ratios between the ambient dose values measured with the active dosimeter and those scored in FLUKA, the proton beam intensities are slightly different from the intensity for the measurements with passive dosimeters. This difference however should not influence the measurements due to e.g., saturation or other effects. As can be seen the both types of neutron dosimeters show a very good agreement with FLUKA simulations and are within 30 % uncertainty allowed for the radiation measurement devices.

2025 JINST 20 P12014

Table 2. Result of the ambient dose measurement with passive and active dosimeters and comparison to the simulation results of the ambient dose equivalent scoring in FLUKA for 1.78e11 protons impinging Moon regolith substitute target.

1	position	0	1	2	3	4
2	GSI ball [µSv]	292,61	292,08	269,33	229,86	161,58
3	FLUKA/neutron [µSv]	392,09	369,29	291,13	256,28	160,22
4	ratio GSI ball	**0,75**	**0,79**	**0,93**	**0,90**	**1,01**
5	ratio Wendi-II	**1,02**	**1,29**	**1,25**	**1,18**	**1,18**
6	GSI cylinder [µSv]	50,59	246,02	259,60	164,02	17,48
7	FLUKA/non-neutron [µSv]	62,74	329,25	367,82	206,29	13,06
8	FLUKA/all-charged [µSv]	58,63	325,04	363,62	201,81	8,69
9	FLUKA/photon [µSv]	4,10	4,22	4,21	4,48	4,37
10	ratio GSI cylinder	**0,81**	**0,75**	**0,71**	**0,80**	**1,34**
11	ratio FHT191	**2,03**	**1,23**	**0,92**	**1,13**	**1,81**

The FLUKA results are assumed here as reference values, though of course uncertainty of the physical models or simple geometrical uncertainties of the positions can vary the neutron ambient dose value. However, in this case the measurements with approved and reliable devices showed FLUKA to be a perfect tool for secondary radiation investigations on e.g., moon surface.

The ambient doses measured with the passive GSI cylinder dosimeter and those simulated for all charged particles and photons are presented in the sixth and seventh rows of table 2, respectively. The further 8th and 9th rows are the FLUKA-calculated contributions to the ambient dose equivalent from charged particles and gammas separately, as some manufacturers provide response to the gamma radiation only. The experimental conditions are the same, the Moon regolith target bombarded by 1.78e11 protons at 430 MeV. As shown in table 2, the contribution of gammas to the ambient dose is relatively low. This is due to the small fluence-to-ambient dose conversion (see, for example, figure 1), though the flux of gammas per cm^2 is essentially higher than of charged particles. We have not found any peculiarities in ambient dose measurements for different positions, thus further tables will provide only the ambient dose (sum) from all particles except of neutrons. The tenth row shows the ratio between the measured, using GSI cylinder, and the simulated ambient doses. It should be noted that the TLDs were read out few days later after the experiment, which is irrelevant for the neutron dose measurements, but provide additional background for non-neutron radiation studies. Reference TLDs were used to estimation the background and recorded a value of 8.3 µSv, which was subtracted from the measured values to yield the final experimental results. The measured ambient doses with values around and especially below 8.3 µSv would provide much higher uncertainties, than typical passive dosimeter studies with error bars around 5–10 %. Nevertheless, the measured non-neutron ambient dose values are again in a very good agreement with FLUKA simulation results.

In the last (11th) row of table 2, the ratios between the active dosimeter measurements and FLUKA simulation results are presented for the ThermoFisher's FHT191N ionization chamber, which is the perfect tool for gamma radiation measurements [16]. The FHT191N response to charged particles is beyond the scope of this paper, and the provided ratios are included for a reference purpose only.

2025 JINST 20 P12014

Table 3. Results of the ambient dose measurements with passive and active dosimeters and comparison to the simulation results of the $H^*(10)$ scoring in FLUKA for 2.2e10 helium (top) and 7.8e9 carbon (bottom) ions impinging Moon regolith substitute target.

1	position	0	1	2	3	4
2	GSI ball [µSv]	1176,9	322,4	175,4	169,2	110,9
3	FLUKA/neutron [µSv]	652,0	378,2	257,8	211,8	117,8
4	ratio GSI ball	**1,8**	**0,9**	**0,7**	**0,8**	**0,9**
5	ratio Wendi-II	**2,8**	**1,2**	**1,1**	**1,0**	**1,0**
6	GSI cylinder [µSv]	541,6	175,4	111,6	71,1	9,2
7	FLUKA/non-neutron [µSv]	763,2	186,3	112,9	61,9	6,0
8	ratio GSI cylinder	**0,7**	**0,9**	**1,0**	**1,1**	**1,5**
9	ratio FHT191	**0,8**	**1,3**	**1,3**	**1,6**	**2,1**

1	position	0	1	2	3	4
2	GSI ball [µSv]	356,5	166,1	96,2	82,0	49,1
3	FLUKA/neutron [µSv]	284,9	197,4	139,1	114,7	65,6
4	ratio GSI ball	**1,3**	**0,8**	**0,7**	**0,7**	**0,7**
5	ratio Wendi-II	**1,6**	**1,2**	**1,1**	**1,0**	**0,9**
6	GSI cylinder [µSv]	145,5	84,3	53,4	37,2	5,0
7	FLUKA/non-neutron [µSv]	184,9	104,7	61,6	34,3	3,6
8	ratio GSI cylinder	**0,8**	**0,8**	**0,9**	**1,1**	**1,4**
9	ratio FHT191	**1,1**	**1,1**	**1,2**	**1,5**	**1,9**

In table 3 one can find the ambient dose values measured with passive dosimeters and calculated for helium-4 and carbon-12 beams with intensities 2.2e10 and 7.8e9 particles, respectively, which also corresponds to approximately 20 spills for each ion specie from the accelerator. It is worth mentioning that the background effects caused by beam losses during extraction, for the helium and carbon beams, as well as for protons, are less than 1 % at the measurement positions and can be neglected. For the He and C beams we have again a good agreement between the neutron ambient dose measurements and simulations, except for the 0° angle. This discrepancy is particularly pronounced for the helium beam, where the measured-to-simulated ambient dose ratio for the GSI ball dosimeter reaches **1.8**. This effect at small angles is known [12] and related to the secondary protons interacting with construction materials, like PE moderator of the GSI ball or Wendi-II dosimeters, generating additional neutrons. However, the folding of secondary proton fluence with the corresponding response of GSI ball dosimeter provides only a small 23.7 µSv addition to the ambient dose value. Further search of particles contributing to neutron signal at 0° reveals a significant fluence of H-2 and H-3 isotopes in the secondary beam, see figure 4. The calculated responses for GSI ball dosimeter to deuterium and tritium beams provided additional signal of 151.2 µSv from deuterium and 347 µSv from tritium, correcting the ratio of the measured to calculated neutron ambient doses to **1.0**. For carbon beam the contribution of spallation fragments to neutron dose in forward direction is visible, but not that pronounced than in case of helium fragmentation. As a result of this study one can propose, that this He-4 fragmentation

2025 JINST 20 P12014

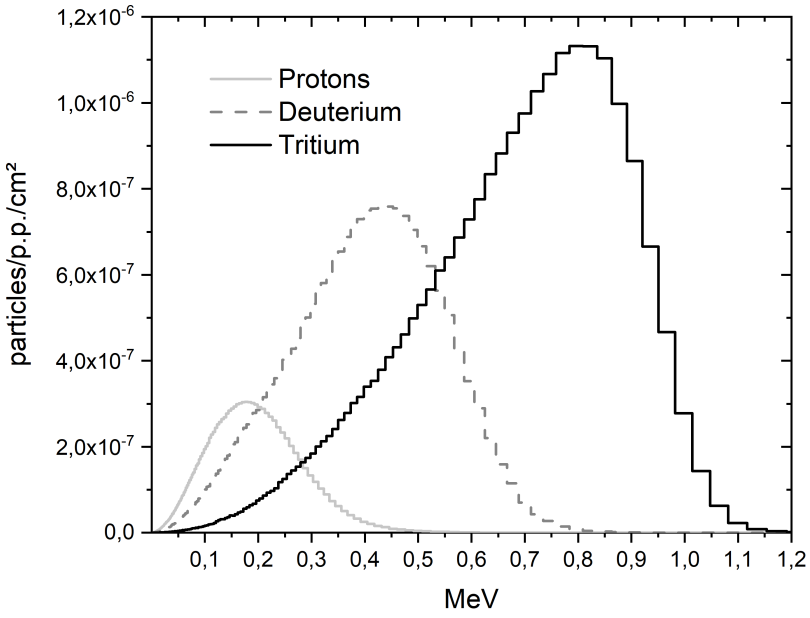

Figure 4. Proton, deuterium and tritium fluences at the position 0° for helium beam impinging Moon regolith substitute target, in units particles per primary beam per cm^2.

from cosmic rays could contribute to the change of the natural amount of deuterium, as well as of He-3 (from tritium decay) under the Moon surface, as it was discussed e.g., in [22].

The measurements with the passive cylinder dosimeters also showed good agreement with the $H^*(10)$ simulation values, except for the large 90° angle, where the dose is comparable or below the background. One should once more mention, that the simulations of the ambient dose in fluka2023.3 include fluence-to-ambient dose conversion for ions like tritium and deuterium as well, approving the capability of the cylinder dosimeter to be suitable for ambient dose measurements of all charged particles.

3.3 Aluminum target

The experimental setup used with aluminium target is the same, with the same angles and distances to the measurement positions relative to the front end of the target. Table 4 presents the results for the proton, helium and carbon beams at 430 MeV/u, with intensities of 1.82e11, 2.5e9 and 1.14e10 particles, respectively. Again, we observe a very good agreement between the measurements and simulations of the ambient neutron dose, see rows 4 and 5 with the ratios for GSI ball and Wendi-II dosimeters. The discrepancy for the 0° angle, where the beam fragments contribute significantly to the neutron dose was discussed in the previous section. The measured with GSI cylinder non-neutron ambient dose values are also in a good agreement with simulations, except for the cases, where the accumulated doses were less or comparable with the background measurements.

The good agreement within nearly 30 % breaks down for the measurements with GSI cylinders on top of the targets, as shown in table 5. Along the projectile path (figure 3), five cylinders were placed on top of each target at nearly equal distances from one another, approximately 23 cm for the Moon regolith substitute and 10 cm for the aluminium target.

2025 JINST 20 P12014

Table 4. Results of the ambient dose measurements with passive and active dosimeters and comparison to the FLUKA simulations, tables from top to the bottom: 1st is for 1.82e11 protons, 2nd for 2.5e9 helium and 3rd for 1.14e10 carbon ions impinging aluminium target.

1	position	0	1	2	3	4
2	GSI ball [µSv]	372	333	237	249	231
3	FLUKA/neutron [µSv]	475	429	324	310	270
4	ratio GSI ball	**0,8**	**0,8**	**0,7**	**0,8**	**0,9**
5	ratio Wendi-II	**1,1**	**1,1**	**1,1**	**1,1**	**1,1**
6	GSI cylinder [µSv]	34,0	32,4	30,6	31,1	15,1
7	FLUKA/non-neutron [µSv]	24,4	23,7	34,8	30,2	9,5
8	ratio GSI cylinder	**1,4**	**1,4**	**0,9**	**1,0**	**1,6**
9	ratio FHT191	**1,8**	**2,0**	**1,4**	**1,5**	**2,0**

1	position	0	1	2	3	4
2	GSI ball [µSv]	155,0	34,6	19,1	19,8	14,5
3	FLUKA/neutron [µSv]	70,8	42,5	28,0	25,0	18,8
4	ratio GSI ball	**2,2**	**0,8**	**0,7**	**0,8**	**0,8**
5	ratio Wendi-II	**2,9**	**1,1**	**1,0**	**1,0**	**1,2**
6	GSI cylinder [µSv]	80,7	12,1	5,0	3,9	2,8
7	FLUKA/non-neutron [µSv]	87,8	11,7	3,3	2,0	0,6
8	ratio GSI cylinder	**0,9**	**1,0**	**1,5**	**2,0**	**4,8**
9	ratio FHT191	**0,9**	**1,5**	**1,7**	**2,0**	**1,8**

1	position	0	1	2	3	4
2	GSI ball [µSv]	510	195	126	118	101
3	FLUKA/neutron [µSv]	423	272	189	175	137
4	ratio GSI ball	**1,2**	**0,7**	**0,7**	**0,7**	**0,7**
5	ratio Wendi-II	**1,9**	**1,1**	**1,0**	**0,9**	**0,9**
6	GSI cylinder [µSv]	217,2	52,1	23,1	20,8	7,5
7	FLUKA/non-neutron [µSv]	281,6	58,9	23,8	15,9	4,5
8	ratio GSI cylinder	**0,8**	**0,9**	**1,0**	**1,3**	**1,7**
9	ratio FHT191	**1,2**	**1,1**	**1,4**	**1,6**	**1,9**

For the moon target, due to some deviations between real and simulated geometry (see section 2.2), a slight discrepancy of the ambient dose values was anticipated. However, for the aluminium target, the considerable overestimation of the non-neutron ambient dose measured with the cylinder dosimeters, compared to the simulations, was not expected. In figure 5, as an example, the calculated fluences of different particles per primary helium ion per unit of lethargy [dF/dln(E)] are shown. The spectra are for the second cylindrical dosimeters on top of the moon and aluminium targets, located approximately 28 and 16 cm from the front surface, respectively. The main contribution to the measured non-neutron dose on top of the moon target is clearly dominated by protons, which have in cylinders high fluence-to-ambient dose conversion coefficients. For the aluminium target, the

2025 JINST 20 P12014

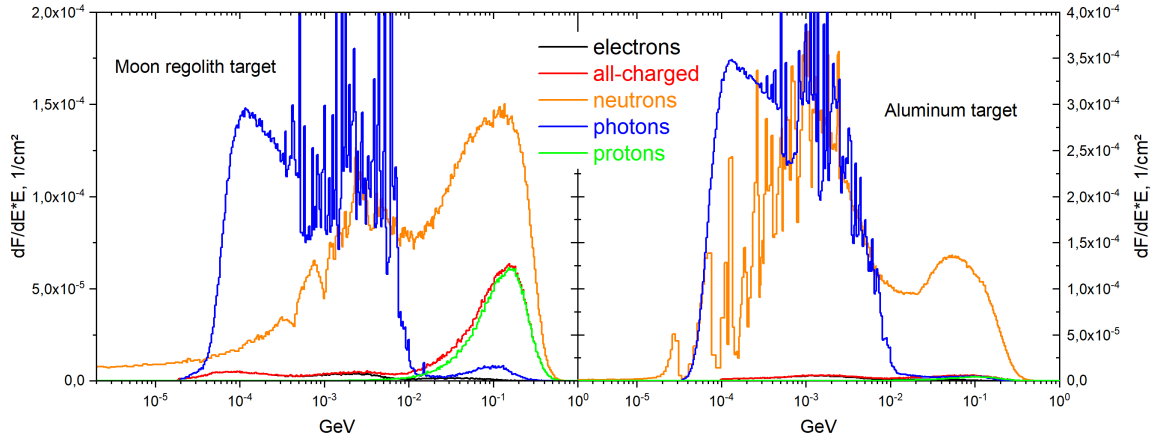

Figure 5. Simulated proton, electron, all-charged particles, photon and neutron fluences for the measurements on top of the Moon regolith substitute (left) and aluminium (right) targets irradiated with He-4 beam at 430 MeV/u.

Table 5. Results of ambient dose measurements with passive cylindrical dosimeters on top of the Moon regolith substitute and aluminum targets (see figure 3, right) for the helium beam, along with a comparison to FLUKA-calculated $H^*(10)$ values. The central positions of the cylindrical dosimeters on the moon target are at approximately 3, 28, 51, 74, 93 cm measured from the front end of the target, corresponding to the 1st, 2nd, 3rd, 4th and 5th positions in the table, respectively. For the aluminum target the 1st to 5th positions of the cylinders' centers are at 3, 16, 26, 36, 46 cm from the front end, facing the beam.

Position from the front end		1st	2nd	3rd	4th	5th
Moon regolith target	measured, µSv	276	2622	3569	2748	1819
	FLUKA sim., µSv	244	3180	4491	3877	2887
	Ratio, meas./sim.	**1,14**	**0,82**	**0,79**	**0,71**	**0,63**
aluminum target	measured, µSv	37,0	104,8	164,7	169,0	136,1
	FLUKA sim., µSv	19,5	54,0	97,0	107,8	88,5
	Ratio, meas./sim.	**1,90**	**1,94**	**1,70**	**1,57**	**1,54**

proton contribution to the non-neutron ambient dose is comparable to that of gammas. This occurs even though the proton (or any other charged particle) fluence is almost negligible compared to the photon fluence (see figure 5), due to the target's higher density and larger effective atomic number. The calculated neutron ambient doses at the positions of the second cylinders for both the moon and Al targets are of the same order of magnitude: 5.7 mSv and 1.2 mSv, respectively. However, in the first case the non-neutron ambient dose makes up 1/3 of the total dose, while for the aluminium target it accounts for only 1/20 of the total dose. Based on our observations and the measured ambient doses, we assume that the passive cylinder dosimeters are also sensitive to neutron radiation, with an empirical neutron response of the same order of magnitude as for photons. Especially the high energy neutron peaks are very close in intensities for both targets and could cause a significant contribution to the gamma dosimeters read-out. This was shown, for example in [23] for ionisation chambers, where the drastical increase in neutron response was calculated and observed for energies above 100 MeV. In case of Moon regolith substitute the neutron contribution seems to be negligible, as the ambient dose measured using cylinder dosimeters was dominated by protons, but for aluminium

2025 JINST 20 P12014

target it increases significantly the read-out values. Also, the sensitivity to neutrons could explain slightly higher measured-to-simulated ambient dose ratios for aluminium target at positions 0 and 1, where the deviation of the ratio is already around 40 %, see table 4.

However, the neutron response simulations for the cylindrical dosimeter using the standard approach of scoring absorbed energy, gives high overestimation for the TLD700 cards readings. The further simulations and response cross-check with measurements, which requires pure neutron fields available only at rare facilities like PTB [11], are the goal for the future study.

4 Summary

The lunar regolith substitute and aluminum targets were irradiated with protons, helium and carbon ions and the ambient doses were measured at different positions around the targets. The simulations with FLUKA were made and different values, like neutron, photon, charged particles $H^*(10)$ values and fluences or spectra were scored.

The neutron ambient dose measurements around the targets using GSI passive neutron dosimeter and commercially available Wendi-II active dosimeter approved the FLUKA calculations. Other way around, FLUKA revealed a necessity of including ion fragments in case of carbon and especially helium beams measurements in forward direction, to correct for a real neutron ambient dose, as the light fragments: protons, deuterons and tritium lead to a strong neutron ambient dose overestimations by the devices.

The passive cylindrical dosimeter was tested at first against the primary proton and helium beams at 200 MeV/u and afterward in the secondary radiation fields around the targets. The measured ambient doses from all particles accept neutrons showed a very good correspondence with FLUKA simulations, which also includes contribution of ions to the radiation field. This, now relatively new feature approved itself to be very useful to calculate the total ambient dose rates. Additionally, the cylinder dosimeter seems to be sensitive to neutrons, which can explain some inconsistencies in case of dominated neutron component in total ambient dose. Still more sophisticated approach, than scoring of the absorbed energy in TLDs, is required to understand the responses of the dosimeter to neutrons.

Most of the measurements using ionization chamber FHT191N, especially where the neutron ambient dose was dominating, showed some overestimations up to a factor of 2, rare underestimations were within 20 %, which is acceptable from radiation safety point of view. Ambient dose overestimations can also mean, as in case of the passive cylindrical dosimeter, the sensitivity to neutrons, though of course a neutron dosimeter, like Wendi-II, is required to get the correct neutron ambient dose equivalent value.

Passive and active dosimeters used in experiment approved themselves as reliable measuring equipment, which in combination with Monte Carlo — FLUKA simulations can provide detailed analysis of complicated radiation fields.

Acknowledgments

This work was supported by the DEIMOS project, which is an ESA CORA (Continuously Open Research Announcement) funded project (Contract nr 4000134861/21/NL/PA/pt).

The authors would like to thank Brons Stephan and Scheloske Stefan for organization and their support during and after the experiments at HIT.

The publication is funded by the Open Access Publishing Fund of GSI Helmholtzzentrum fuer Schwerionenforschung.

2025 JINST 20 P12014

References

[1] http://www.gsi.de.

[2] G. Fehrenbacher et al., *Measurement of the fluence response of the GSI neutron ball dosemeter in the energy range from thermal to 19 MeV*, *Radiat. Prot. Dosimetry* **126** (2007) 546.

[3] L. Jägerhofer et al., *A new method to calculate the response of the WENDI-II rem counter using the FLUKA Monte Carlo Code*, *Nucl. Instrum. Meth. A* **691** (2012) 81.

[4] E. Kozlova et al., *The characterization studies of mixed radiation fields generated by a 1 GeV/u iron beam impinging on a thick aluminum target inside and outside of Cave A at GSI*, to be published.

[5] https://www.thermofisher.com/.

[6] A. Ferrari, P.R. Sala, A. Fasso and J. Ranft, *FLUKA: A multi-particle transport code (Program version 2005)*, CERN-2005-010 (2005) [DOI:10.2172/877507].

[7] F. Ballarini et al., *FLUKA: status and perspectives*, in the proceedings of the *15th Workshop on Shielding Aspects of Accelerators, Targets, and Irradiation Facilities*, East Lansing, Michigan, U.S.A., September 20-23, 2022, in press.

[8] S.E. Combs, O. Jäkel, T. Haberer and J. Debus, *Particle therapy at the Heidelberg Ion Therapy Center (HIT) — Integrated research-driven university-hospital-based radiation oncology service in Heidelberg, Germany*, *Radiother. Oncol.* **95** (2010) 41.

[9] A. Di Chicco et al., *Characterization of the secondary neutron field produced by 430 MeV/u proton, ^{4}He, and ^{12}C beams incident on blocks of lunar regolith simulant*, in the proceedings of the *45th COSPAR Scientific Assembly*, Busan, South Korea, July 13–21 (2024), p. 2193.

[10] F. Luoni et al., *Dose Build-up of High-energy 1H and 4He Ions in Standard, Innovative and In Situ Shielding Materials for Space Radiation: Measurements and Simulations*, *Radiat. Res.* **203** (2025) 163.

[11] R. Nolte et al., *Quasi-monoenergetic neutron reference fields in the energy range from thermal to 200 MeV*, *Radiat. Prot. Dosimetry* **110** (2004) 97.

[12] D. Boscolo et al., *Characterization of the Secondary Neutron Field Produced in a Thick Aluminum Shield by 1 GeV/u 56Fe Ions Using TLD-Based Ambient Dosimeters*, *Front. Phys.* **8** (2020) 365.

[13] G. Fehrenbacher et al., *Neutron dose measurements with the GSI ball at high-energy accelerators*, *Radiat. Prot. Dosimetry* **125** (2007) 209.

[14] A. Sokolov et al., *Neutron spectra at a high energy heavy ion accelerator measured with a TLD-based Bonner spectrometer*, 2021 *JINST* **16** P10022.

[15] M. Pelliccioni, *Overview of Fluence-to-Effective Dose and Fluence-to-Ambient Dose Equivalent Conversion Coefficients for High Energy Radiation Calculated Using the FLUKA Code*, *Radiat. Prot. Dosimetry* **88** (2000) 279.

[16] https://assets.thermofisher.com/TFS-Assets/LSG/Specification-Sheets/D10458~.pdf.

[17] A.M. Hillas, *Cosmic Rays*, The Commonwealth and International Library: Selected Readings in Physics (1972).

[18] G.D. Badhwar and P.M. O'Neill, *Galactic cosmic radiation model and its applications*, *Adv. Space Res.* **17** (1996) 7.

[19] https://www.offplanetresearch.com.

[20] F. Horst et al., *Thick shielding against galactic cosmic radiation: A Monte Carlo study with focus on the role of secondary neutrons*, *Life Sciences in Space Research* **33** (2022) 58.

2025 JINST 20 P12014

[21] V. Vlachoudis, *Flair: A powerful but user friendly graphical interface for FLUKA*, in the proceedings of the *International Conference on Mathematics, Computational Methods & Reactor Physics*, Saratoga Springs, NY, U.S.A., May 3–7 (2009).

[22] E. Füri, E. Deloule and R. Trappitsch, *The production rate of cosmogenic deuterium at the Moon's surface*, *Earth Planet. Sci. Lett.* **474** (2017) 76.

[23] C. Theis et al., *Field calibration studies for ionisation chambers in mixed high-energy radiation fields*, *Radiat. Prot. Dosimetry* **126** (2007) 299.

2025 JINST 20 P12014